A recurrent COL6A1 pseudoexon insertion causes muscular dystrophy and is effectively targeted by splice-correction therapies

Véronique Bolduc, A. Reghan Reghan Foley, Herimela Solomon-Degefa, Apurva Sarathy, Sandra Donkervoort, Ying Hu, Grace S Chen, Katherine Sizov, Matthew Nalls, Haiyan Zhou, et al.

JCI insight

A recurrent *COL6A1* pseudoexon insertion causes muscular dystrophy and is effectively targeted by splice-correction therapies

Véronique Bolduc, … , Francesco Muntoni, Carsten G. Bönnemann

JCI Insight. 2019;4(6):e124403. https://doi.org/10.1172/jci.insight.124403.

Research Article | Muscle biology | Therapeutics

The clinical application of advanced next-generation sequencing technologies is increasingly uncovering novel classes of mutations that may serve as potential targets for precision medicine therapeutics. Here, we show that a deep intronic splice defect in the *COL6A1* gene, originally discovered by applying muscle RNA sequencing in patients with clinical findings of collagen VI–related dystrophy (COL6-RD), inserts an in-frame pseudoexon into *COL6A1* mRNA, encodes a mutant collagen α1(VI) protein that exerts a dominant-negative effect on collagen VI matrix assembly, and provides a unique opportunity for splice-correction approaches aimed at restoring normal gene expression. Using splice-modulating antisense oligomers, we efficiently skipped the pseudoexon in patient-derived fibroblast cultures and restored a wild-type matrix. Similarly, we used CRISPR/Cas9 to precisely delete an intronic sequence containing the pseudoexon and efficiently abolish its inclusion while preserving wild-type splicing. Considering that this splice defect is emerging as one of the single most frequent mutations in COL6-RD, the design of specific and effective splice-correction therapies offers a promising path for clinical translation.

JCI insight

RESEARCH ARTICLE

A recurrent *COL6A1* pseudoexon insertion causes muscular dystrophy and is effectively targeted by splice-correction therapies

Véronique Bolduc,[1] A. Reghan Foley,[1] Herimela Solomon-Degefa,[2] Apurva Sarathy,[1] Sandra Donkervoort,[1] Ying Hu,[1] Grace S. Chen,[1] Katherine Sizov,[1] Matthew Nalls,[1] Haiyan Zhou,[3,4] Sara Aguti,[3] Beryl B. Cummings,[5,6] Monkol Lek,[5] Taru Tukiainen,[5,6] Jamie L. Marshall,[6] Oded Regev,[7] Dina Marek-Yagel,[8] Anna Sarkozy,[3] Russell J. Butterfield,[9] Cristina Jou,[10,11,12] Cecilia Jimenez-Mallebrera,[11,12] Yan Li,[13] Corine Gartioux,[14] Kamel Mamchaoui,[14] Valérie Allamand,[14] Francesca Gualandi,[15] Alessandra Ferlini,[3,15] Eric Hanssen,[16] the *COL6A1* Intron 11 Study Group,[17] Steve D. Wilton,[18,19] Shireen R. Lamandé,[20,21] Daniel G. MacArthur,[5,6] Raimund Wagener,[2] Francesco Muntoni,[3,22] and Carsten G. Bönnemann[1]

[1]Neuromuscular and Neurogenetic Disorders of Childhood Section, National Institute of Neurological Disorders and Stroke, NIH, Bethesda, Maryland, USA. [2]Center for Biochemistry, Faculty of Medicine and Center for Molecular Medicine Cologne, University of Cologne, Cologne, Germany. [3]Dubowitz Neuromuscular Centre, UCL Institute of Child Health & Great Ormond Street Hospital for Children, London, United Kingdom. [4]Genetics and Genomic Medicine Programme, UCL Great Ormond Street Institute of Child Health, London, United Kingdom. [5]Analytical and Translation Genetics Unit, Massachusetts General Hospital, Boston, Massachusetts, USA. [6]Medical and Population Genetics, Broad Institute of MIT and Harvard, Cambridge, Massachusetts, USA. [7]Courant Institute of Mathematical Sciences, New York University, New York, USA. [8]Metabolic Disease Unit, Edmond and Lily Safra Children's Hospital, Sheba Medical Center, Tel-Hashomer, Israel. [9]Department of Neurology and Pediatrics, University of Utah, Salt Lake City, Utah, USA. [10]Pathology Department and Biobanc de l'Hospital Infantil Sant Joan de Déu per a la Investigació, Hospital Sant Joan de Déu, Barcelona, Spain. [11]Neuromuscular Unit, Neuropediatrics Department, Hospital Sant Joan de Déu, Institut de Recerca Sant Joan de Déu, Esplugues de Llobregat, Barcelona, Spain. [12]CIBERER (ISCIII), Madrid, Spain. [13]Peptide/Protein Sequencing Facility, National Institute of Neurological Disorder and Stroke, NIH, Bethesda, Maryland, USA. [14]Sorbonne Université, Inserm, Association Institut de Myologie, Centre de Recherche en Myologie, UMRS974, Paris, France. [15]Medical Genetics Unit, Department of Medical Science, University of Ferrara, Ferrara, Italy. [16]Bio21 Advanced Microscopy Facility, The University of Melbourne, Melbourne, Australia. [17]The *COL6A1* Intron 11 Study Group is detailed in the Supplemental Acknowledgments. [18]Centre for Molecular Medicine and Therapeutics, Murdoch University, Perth, Australia. [19]Perron Institute for Neurological and Translational Science, University of Western Australia, Perth, Australia. [20]Murdoch Children's Research Institute, Parkville, Australia. [21]Department of Paediatrics, University of Melbourne, Parkville, Australia. [22]NIHR Great Ormond Street Hospital Biomedical Research Centre, London, United Kingdom.

The clinical application of advanced next-generation sequencing technologies is increasingly uncovering novel classes of mutations that may serve as potential targets for precision medicine therapeutics. Here, we show that a deep intronic splice defect in the *COL6A1* gene, originally discovered by applying muscle RNA sequencing in patients with clinical findings of collagen VI–related dystrophy (COL6-RD), inserts an in-frame pseudoexon into *COL6A1* mRNA, encodes a mutant collagen α1(VI) protein that exerts a dominant-negative effect on collagen VI matrix assembly, and provides a unique opportunity for splice-correction approaches aimed at restoring normal gene expression. Using splice-modulating antisense oligomers, we efficiently skipped the pseudoexon in patient-derived fibroblast cultures and restored a wild-type matrix. Similarly, we used CRISPR/Cas9 to precisely delete an intronic sequence containing the pseudoexon and efficiently abolish its inclusion while preserving wild-type splicing. Considering that this splice defect is emerging as one of the single most frequent mutations in COL6-RD, the design of specific and effective splice-correction therapies offers a promising path for clinical translation.

Authorship note: ARF, HSD, and A. Sarathy contributed equally to this work.

Conflict of interest: CGB, VB, FM, BBC, ML, DGM, and SDW share a patent related to the diagnosis of the mutation described in this study, and to a method for treating it (PCT/US2017/040726 - WO 2018/009547 A1). DGM is a founder with equity in Goldfinch Bio, and has received research support from Biogen, Merck, Pfizer, Eisai, BioMarin, and Alnylam.

Submitted: September 4, 2018
Accepted: February 12, 2019
Published: March 21, 2019.

Reference information: JCI Insight. 2019;4(6):e124403. https://doi.org/10.1172/jci.insight.124403.

Introduction

Collagen VI–related dystrophies (COL6-RDs) are extracellular matrix disorders, affecting skeletal muscle and connective tissues and ranging in phenotypic severity from the severe Ullrich congenital muscular dystrophy (UCMD), through intermediate phenotypes, to the milder Bethlem myopathy (reviewed in ref. 1). Clinical manifestations include muscle weakness, distal joint hyperlaxity, proximal joint contractures, scoliosis, and progressive respiratory insufficiency. COL6-RDs are among the most common congenital muscular dystrophy subtypes (1–4), and while supportive interventions such as nocturnal noninvasive ventilation have improved survival considerably (5, 6), there are no specific therapeutic interventions.

Collagen type VI synthesis, secretion, and assembly in the extracellular space is a complex, stepwise process mediated by the collagen-synthesizing tissue-resident fibroblast populations (7, 8). The 3 major disease-related *COL6* genes (*COL6A1*, *COL6A2*, and *COL6A3*) encode 3 polypeptide chains [α1(VI), α2(VI), and α3(VI)] that are necessary for collagen VI production. Each of the 3 chains is composed of a short central collagenous triple helical domain, distinguishable by the presence of uninterrupted Gly-X-Y repeats, that is flanked by globular domains. The triple helical domains enable the α1(VI), α2(VI), and α3(VI) chains to intertwine and form a heterotrimeric α1-α2-α3 monomer. Monomers join laterally to form staggered antiparallel dimers, which then associate in parallel to form a 112-nm-long tetramer. The tetramers are subsequently secreted into the extracellular space where they form higher-order structures by end-to-end association and branching (9–14). Functional collagen VI is a connected meshwork of tetramers, ultrastructurally appearing as beaded microfibrils (15).

Mutations in *COL6A1*, *COL6A2*, and *COL6A3* cause COL6-RD and act in a recessive or dominant fashion, with de novo dominant-negative mutations emerging as the most prevalent mutation type across the phenotypic spectrum (1, 16–19). These mutations are in-frame exon skipping mutations or glycine missense mutations in the triple helical Gly-X-Y motifs and occur preferentially at the N-terminal end of the respective triple helical domains (14, 16, 20, 21). Formation of the triple helix comprising the 3 α chains proceeds from the C- to the N-terminal end; therefore, chains carrying a mutation located towards their N-terminus can result in a helix stable enough to retain the mutant chain in the α1-α2-α3 monomer. If monomers incorporating a mutant chain are then carried forward to reach the tetrameric state, 15 out of 16 nascent tetramers contain at least one mutant chain, resulting in pervasive disturbance of collagen VI matrix assembly and function (14, 16).

Recently, as part of a large study exploring the utility of muscle RNA sequencing as a diagnostic tool in neuromuscular disorders, we uncovered an in-frame pseudoexon retention in *COL6A1* that mapped at the N-terminal end of the triple helical domain of the α1(VI) chain, in 4 unrelated patients with a clinical and pathological phenotype highly suggestive of COL6-RD (22). Parallel whole-genome sequencing in all 4 patients identified a de novo heterozygous deep intronic variant (c.930+189C>T, hereafter referred as +189C>T) creating the donor splice site activating the pseudoexon insertion (22). Our initial screening for the +189C>T mutation in international COL6-RD cohorts resulted in the identification of 27 additional patients harboring the +189C>T mutation (22), thus revealing +189C>T as an unexpectedly common causative mutation for COL6-RD.

Mutations activating pseudoexons such as the one described here are excellent targets for splice-correction interventions. In particular, the skipping of pathogenic pseudoexons by antisense-mediated oligomers has been validated in cultured patient-derived cells in a wide range of clinical scenarios, to rescue loss-of-function mutations (23–29). Splice-modulating antisense oligomers are short, single-stranded, chemically modified oligonucleotides, rationally designed to specifically recognize and hybridize to precursor messenger RNA (pre-mRNA) through Watson-Crick base pairing, and consequently interfere with steps of its maturation, such as splicing. Phosphorodiamidate morpholino oligomers (PMOs) and 2′-*O*-methyl–modified bases on a phosphorothioate backbone (2′OMe) are 2 antisense chemistries developed to increase oligomer stability and affinity, and both have been successfully used to promote exon skipping in vitro and in vivo (30–32). Considering that 2 splice-modulating therapeutic antisense oligomers have been recently approved by the US Food & Drug Administration (FDA), namely a PMO for treating a subset of Duchenne muscular dystrophy patients carrying deletions for which the antisense therapy restores the reading frame after dystrophin (*DMD*) exon 51 skipping (33, 34), and a 2′-*O*-methoxyethyl (MOE) phosphorothioate oligomer for spinal muscular atrophy that promotes inclusion of *SMN2* exon 7 (35, 36), developing this

approach for COL6-RD has high translational potential. In the case of this dominantly acting mutation and in contrast to Duchenne muscular dystrophy, successful pseudoexon skipping results in normal transcripts from the mutant allele, with the potential to fully restore normal *COL6A1* expression.

Recently, gene editing via the clustered regularly interspaced short palindromic repeats (CRISPR)/CRISPR-associated protein 9 (Cas9) system has also been exploited to address exon skipping. In this system, a single RNA molecule (guide RNA or gRNA) recruits an endonuclease (Cas9) to a specific genomic locus to induce a double-stranded break, provided that a protospacer-adjacent motif (PAM) is present adjacent to the targeted site. Following cleavage, gDNA is repaired either through homology-directed repair, or, if no template DNA is present to carry out homology-directed repair, through a nonhomologous end-joining process that is prone to introducing random insertion/deletion mutations (indels) at the site of repair (37). Skipping of exons by CRISPR/Cas9 can be accomplished using a dual-gRNA strategy, where targeting each flanking intron of the exon to be spliced out with a gRNA leads to the genomic excision of the targeted exon and its exclusion from the final mRNA product. This approach has been successfully used to reframe several deletion and truncating mutations in the *DMD* gene, where deleting up to 11 additional consecutive exons allowed the restoration of the reading frame and expression of a partially functional internally deleted dystrophin (38–44). Furthermore, deep intronic mutations are especially amenable to dual-gRNA excision strategies in the case of pathogenic recessive (45, 46) or dominantly acting mutations, as small deletions in introns are predicted to mostly spare the normal splicing patterns within the targeted gene.

Here, we further extend the cohort of *COL6A1* +189C>T mutation–positive patients who we find present with an unusually progressive clinical course. We investigate the functional consequences of the +189C>T mutation for splicing and show that the mutant α1 chain carrying the pseudoexon sequence is translated and secreted, interfering with collagen VI matrix assembly. We identify specific splice-modulating oligomers capable of effectively skipping the abnormal splicing product induced by this mutation and restoring a wild-type (WT) matrix phenotype in cultured cells. We show that deleting an intronic fragment encompassing the site of the deep intronic splice-activating mutation along with the pseudoexon sequence efficiently restores normal splicing from the mutant allele without affecting the normal allele.

Results

Screening for the COL6A1 +189C>T mutation. In Cummings et al. (22), we initially reported a pseudoexon insertion in RNA sequencing reads from muscle specimens of 4 index patients (US1, US2, UK1, and UK2; corresponding to N31, N32, N29, and N30, respectively; see ref. 22) with clinical phenotypes and muscle imaging highly suggestive of COL6-RD, muscle immunohistochemical findings of mislocalized collagen VI (Figure 1A), and who were previously negative for directed *COL6* mutation testing and whole-exome sequencing. The splice-gain event inserts a 72-nt pseudoexonic sequence between *COL6A1* exons 11 and 12 (22) (Figure 1B). Subsequent whole-genome sequencing showed that all 4 patients carried a de novo deep intronic heterozygous change at the pseudoexon junction (NM_001848 c.930+189C>T; Figure 1C) (22). This *COL6A1* +189C>T mutation is predicted to create a consensus site for the pseudoexon 5′ splice donor (SD) site (aggc>AGgt), and thus to trigger its insertion, using a cryptic signal located upstream as splice acceptor (SA) site (agAC, Figure 1D). Presence of the 72-nt pseudoexon inclusion was verified by reverse transcription PCR (RT-PCR) in both muscle specimens and cultured dermal fibroblasts of patients (22), and was further verified by Sanger sequencing (Supplemental Figure 1; supplemental material available online with this article; https://doi.org/10.1172/jci.insight.124403DS1). See complete unedited blots in the supplemental material.

Since our initial identification of the *COL6A1* +189C>T mutation, we sought to determine whether it constitutes a recurrent mutational mechanism in COL6-RD. We screened mutation-negative COL6-RD–like patients using targeted genomic DNA sequencing, and identified 31 additional cases harboring the *COL6A1* +189C>T mutation (27 of whom were reported in Cummings et al., ref. 22; Supplemental Table 1). Consistent with findings in the 4 index cases, the mutation arose de novo in all cases in which segregation could be verified (20 of 20 families screened, Figure 1C).

Clinical manifestations associated with the COL6A1 +189C>T mutation. Upon review of early clinical manifestations and timing of first concerns for the 35 cases, it was notable that there was a relative paucity of prominent neonatal symptoms in most patients (Supplemental Table 1), which contrasts with the classical UCMD phenotype (1, 47–49). Patients with the *COL6A1* +189C>T mutation, however, uniformly progressed in severity to match typical UCMD, with loss of ambulation and full-time wheelchair use on aver-

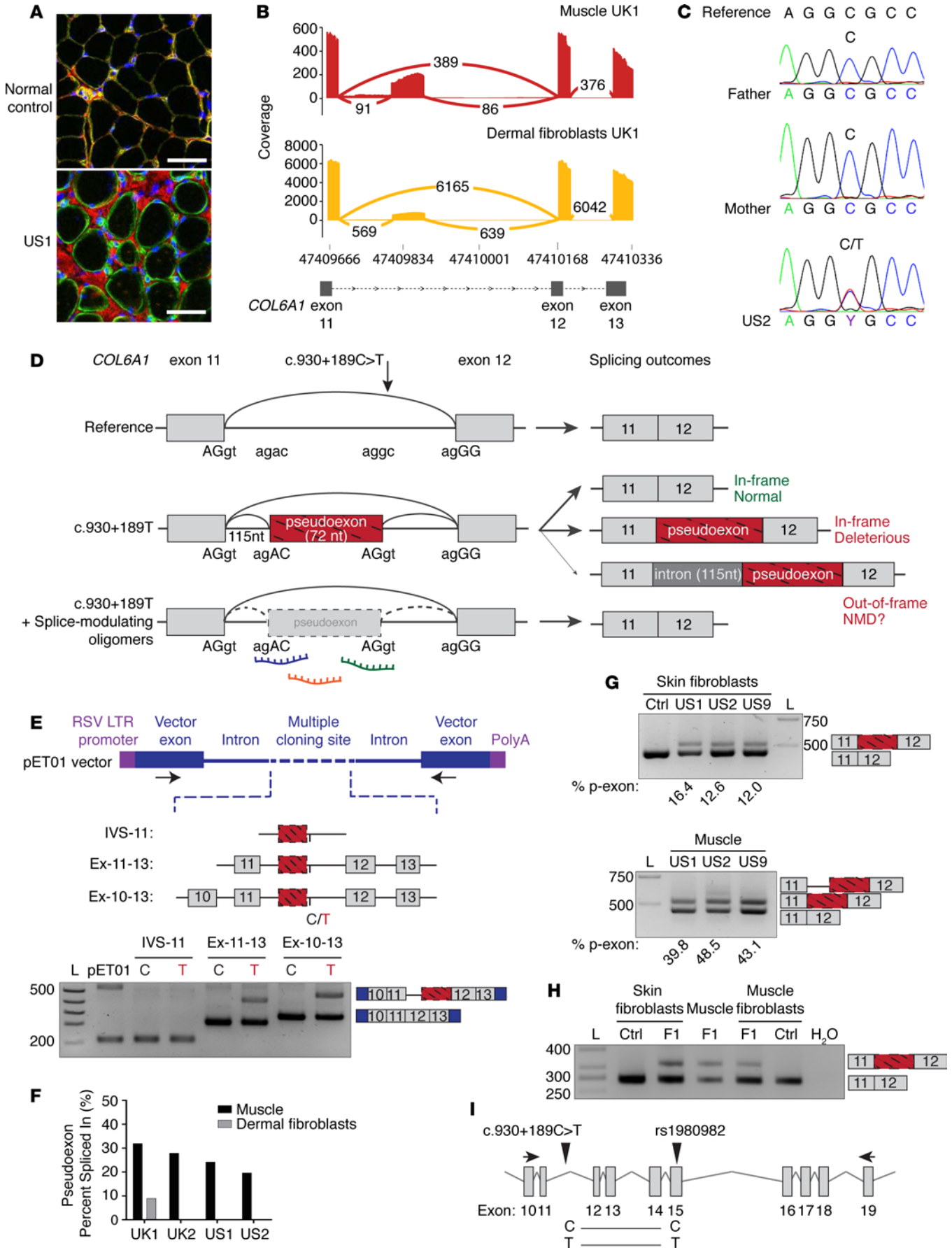
A
Normal control
US1
B
Muscle UK1
Coverage
600
400
200
0
389
376
91
86
Dermal fibroblasts UK1
8000
6000
4000
2000
0
6165
6042
569
639
47409666 47409834 47410001 47410168 47410336
COL6A1 exon 11
exon 12
exon 13
C
Reference A G G C G C C
C
Father A G G C G C C
C
Mother A G G C G C C
C/T
US2 A G G Y G C C
D
COL6A1 exon 11
c.930+189C>T
exon 12
Splicing outcomes
Reference
AGgt agac aggc agGG
11 12
c.930+189T
115nt
pseudoexon (72 nt)
AGgt agAC AGgt agGG
11 12
In-frame Normal
11 pseudoexon 12
In-frame Deleterious
11 intron (115nt) pseudoexon 12
Out-of-frame NMD?
c.930+189T + Splice-modulating oligomers
pseudoexon
AGgt agAC AGgt agGG
11 12
E
RSV LTR promoter
Vector exon
Intron
Multiple cloning site
Intron
Vector exon
PolyA
pET01 vector
IVS-11:
Ex-11-13:
Ex-10-13:
10 11 12 13
C/T
IVS-11
Ex-11-13
Ex-10-13
L pET01 C T C T C T
500
200
10 11 12 13
10 11 12 13
F
Pseudoexon Percent Spliced In (%)
50
40
30
20
10
0
Muscle
Dermal fibroblasts
UK1 UK2 US1 US2
G
Skin fibroblasts
Ctrl US1 US2 US9 L
750
500
11 12
11 12
% p-exon:
16.4 12.6 12.0
Muscle
L US1 US2 US9
750
500
11 12
11 12
11 12
% p-exon:
39.8 48.5 43.1
H
Skin fibroblasts
Muscle
Muscle fibroblasts
L Ctrl F1 F1 F1 Ctrl H2O
400
300
250
11 12
11 12
I
c.930+189C>T
rs1980982
Exon: 1011 12 13 14 15 16 17 18 19
C
T
C
T

Figure 1. A deep intronic *COL6A1* mutation creates a donor splice site, prompting the insertion of a pseudoexonic sequence. (**A**) Immunofluorescence images of muscle biopsy sections of patient US1 and one unaffected control costained for collagen VI (red), basement membrane marker laminin (green), and with nuclear stain DAPI (blue). Scale bars: 50 μm. (**B**) Sashimi plots comparing skeletal muscle biopsy (top) and cultured dermal fibroblast (bottom) RNA sequencing reads from patient UK1, at the *COL6A1* intron 11 locus. (**C**) Genomic DNA chromatograms for the *COL6A1* +189C>T mutation testing in family US2. (**D**) Schematics of the *COL6A1* +189C>T mutation locus depicting the pseudoexon sequence boundaries, and splicing outcomes. Splice-modulating antisense oligomers targeting the pseudoexon pre-mRNA sequence are used to promote its skipping as a therapeutic strategy. (**E**) Splicing reporter (minigene) constructs were prepared by subcloning various segments of *COL6A1* genomic DNA (intervening sequence 11 [IVS-11], exons 11 to 13 [Ex-11-13], or exons 10 to 13 [Ex-10-13]) into the pET01 vector (top). Minigenes were transfected into HEK293T cells, and RNA was isolated 24 hours later. Electrophoretic gel image (bottom) represents reverse transcription PCR (RT-PCR) products, amplified using pET01 primers (arrows). Composition of the amplicons is exemplified for Ex-10-13 (right). L = molecular weight ladder. Gel representative of 3 transfections. (**F**) The pseudoexon percent spliced in (PSI) index was calculated from the RNA sequencing data of 4 muscle specimens and 1 dermis-derived cultured fibroblast specimen, and indicates the percentage of *COL6A1* transcript reads that include the pseudoexon. (**G** and **H**) Detection of the 72-nucleotide pseudoexon expression in 3 cultured dermal fibroblasts and their corresponding muscle biopsy specimens (**G**), or in patient F1's muscle biopsy, cultured dermis- and muscle-derived fibroblasts (**H**), using RT-PCR. Primers spanning *COL6A1* exons 10 to 20 (**G**), or exons 10 to 15 (**H**) were used for amplification. RT-PCR gel images were quantified by densitometry (ImageJ) to determine the percentage pseudoexon expression (% p-exon, indicated below each lane and representing the average of 3 to 4 gel quantifications). (**I**) Location of the single-nucleotide polymorphism rs1980982 relative to the +189C>T mutation site. cDNA from US14 fibroblasts, in whom the "T" allele of rs1980982 is located *in cis* to the +189T mutation (below), was amplified with primers located in exons 10 and 19 (arrows) for subsequent shotgun cloning.

age by the age of 9 years (3–14 years), respiratory insufficiency requiring nocturnal noninvasive ventilation starting on average at the age of 13 years (7–21 years), scoliosis, and development of proximal contractures while maintaining distal joint hypermobility (Supplemental Figure 2 and Supplemental Table 1). Thus, the accelerating evolution of the disease in *COL6A1* +189C>T patients from relatively few clinical findings in the neonatal period to a typically severe UCMD phenotype suggests a strong dominant-negative mechanism of action, which appears to be more pronounced even when compared with other dominantly acting mutations in the *COL6* genes. Immunohistofluorescence performed on muscle biopsy sections revealed a lack of colocalization of collagen VI immunoreactivity to the basement membrane (Figure 1A), as is typically seen in COL6-RD patients with dominant-negative mutations (14).

Splicing profile of the COL6A1 +189C>T mutation. We established a functional splicing assay in HEK293T cells expressing splicing reporter (minigene) constructs that harbored either the C (reference) or the T (mutant) allele, and analyzed the splicing profiles by RT-PCR (Figure 1E). The constructs harbored no variant other than the +189C>T, as verified by Sanger sequencing, such that any variation in splicing can be attributed to the mutation. While the +189C>T indeed created a 5′SD and prompted a splice-gain event in the minigenes encompassing exons 11 to 13 (Ex-11-13) and exons 10 to 13 (Ex-10-13) (Figure 1E), the pseudoexon 3′SA site (that defines the 72-nt insertion) was not utilized in this system. Rather, the natural 3′SA of exon 11 was used, resulting in a 187-nt insertion (115 nt of intron 11 sequence plus 72 nt of pseudoexon sequence), as verified by sequencing the gel-extracted PCR fragments. In contrast, the construct carrying intron 11 sequence only (IVS-11) did not produce any splice gain (Figure 1E). Notably, minigenes harboring the T allele in addition returned normally spliced products as the most abundant splicing outcome (Figure 1E). Together these data validate that the +189C>T mutation is responsible for the pseudoexon insertion, but suggest that the mutation is leaky. In addition, these data suggest that the factors contributing to the pseudoexon 3′SA recognition are not sufficiently present in the exogenously expressed minigenes and may include additional *cis* elements stabilizing the 3′SA further upstream or downstream, or additional splicing factors not present in HEK293T cells.

We then quantified pseudoexon inclusion in various available specimens, including cultured dermal fibroblasts. Dermal fibroblasts are readily accessible, can be expanded in culture, and express high levels of the 3 main *COL6* genes, and thus serve as a valid model to study COL6-RD in vitro (7). The pseudoexon percent spliced in (PSI), calculated using the RNA sequencing data (50), was on average 26.0% of total *COL6A1* in muscle specimens (19.7%–32.0%, $n = 4$), but only 9.0% for one corresponding cultured dermal fibroblast sample (Figure 1, B and F), lower than the 50% expected in the context of heterozygosity without mosaicism (Figure 1C). Using endpoint RT-PCR, we similarly observed lower-than-expected pseudoexon expression in muscle specimens (39.8%–48.5%, Figure 1G), with again lower levels in cultured dermal fibroblasts (10.8%–18.8%, Figure 1G and Supplemental Figure 3). In one patient (F1) for whom muscle-derived fibroblasts were available, the pseudoexon expression was notably lower in cultured muscle-derived fibroblasts (9.8%), than in the fresh muscle specimen (27.5%) (Figure 1H). Together, these data suggest that the process of growing primary cells in vitro alters the splicing efficiency of this pseudoexon, or favors cells capable of splicing it out.

To determine the splicing outcomes of the pre-mRNA transcribed from the mutant allele only, we first identified one patient (US14) carrying an exonic polymorphism (rs1980982 T>C) in close proximity to the pseudoexon inclusion site (Figure 1I), in whom the rs1980982 T allele and the +189T alleles were in phase with the +189T mutation. Shotgun cloning of US14 dermal fibroblast–derived RT-PCR products, followed by sequencing of individual colonies, indicated that 2 mRNA species were produced in similar abundance from the +189T allele in these fibroblasts, that either included the pseudoexon or did not (Supplemental Table 2). Next, careful examination of RT-PCR gel electrophoresis from muscle-derived samples suggested the presence of an additional splice variant of higher molecular weight (Figure 1G, visible in the muscle US2 lane). Upon shotgun cloning and sequencing of US2 muscle–derived RT-PCR products, we identified a third splice product, of low abundance, in which the mutant 5′SD was utilized in combination with the natural 3′SA of the preceding exon 11 (Figure 1D), similar to the splice-gain products identified in the splicing reporter assays (Figure 1E). This splice variant encodes a premature termination codon. In summary, 3 distinct mRNA species originate from pre-mRNA transcripts harboring the mutant +189T allele: a normally spliced variant, an in-frame (72 bp) pseudoexon-containing variant, and, as a rare event in muscle tissue, an out-of-frame intronic insertion likely subject to mRNA decay (Figure 1D).

Effect of the pseudoexon peptide insertion on collagen VI matrix assembly. The pseudoexon peptide, if translated, interrupts the Gly-X-Y repeats with a noncollagenous 24–amino acid sequence at the N-terminal end of the triple helical domain of the α1(VI) chain (Figure 2A), the region in which most of the dominant-negative mutations causing COL6-RD reside (16, 17, 20, 21). To detect expression and secretion of the pseudoexon peptide, we immunoprecipitated collagen VI from dermal fibroblast cell medium (secreted fraction) and lysates (cellular fraction), size-selected the protein fractions (by gel-extracting proteins within the 117–171 kDa range), and performed liquid chromatography–tandem mass spectrometry analysis. When using trypsin as the digestion enzyme, we confidently detected a peptide (RPLHLEGQGQPPR) that was unique to the patient sample (US8), and that was identified in both the cellular and secreted fractions (Table 1 and Supplemental Figure 4). The sequence of this peptide corresponds to a fragment of the predicted translated pseudoexon (Figure 2A). When using chymotrypsin, we similarly detected an overlapping peptide (HLEGQGQPPRHPA) in the patient cellular fraction (Table 1), while we did not detect any mutant peptide in the secreted fraction (possibly due to relatively low specificity of the chymotrypsin digestion).

Using the predicted pseudoexon sequence, we produced an immunizing peptide and raised a polyclonal antibody [Pex11-α1(VI)] against the translated pseudoexon. On denaturing and reducing immunoblots, this pseudoexon-specific antibody detected a strong distinctive band in US8 and IR1 cellular and secreted fractions, at the approximate size for α1(VI) collagen (~130 kDa), while no band of this molecular weight was detected in Ctrl1 fractions, or when probing with the preimmune sera (Figure 2B). Membranes that were first probed with Pex11-α1(VI), then stripped and reprobed with an α1(VI) collagen antibody, confirmed that the Pex11-α1(VI) signal corresponded to the same molecular weight as α1(VI) collagen (Figure 2C). Moreover, the posttranslational modifications that increase the molecular weight of the α1(VI) collagen chain in the secreted fraction seem unaffected by the presence of the pseudoexon (Figure 2C). Together with the mass spectrometry data, the pseudoexon-specific immunoblot detection in both intracellular and secreted fractions provides evidence that the mutant α1(VI) chain (containing the pseudoexonic peptide) is expressed and secreted.

Using negative-staining electron microscopy of secreted proteins, we measured the microfibrillar length (calculated as the number of tetramers per continuous microfibril), which was significantly lower in patients' samples compared with the normal sample (Figure 2D). Visual assessment of immunostaining images also revealed morphological differences in the collagen VI microfibril architecture, which appeared discontinuous and kinked (Figure 2E). Taken together, these observations point to a dominant-negative effect of the mutant pseudoexon on collagen VI matrix assembly.

Skipping of the COL6A1 pseudoexon with antisense oligomers. To direct splicing outcomes from the *COL6A1* +189T–transcribed pre-mRNA in favor of normal transcripts, we first devised a pseudoexon-skipping strategy using antisense oligomers (Figure 1D). We designed PMO and 2′OMe antisense oligomers targeting either the splice junctions (SA or SD) or pseudoexon internal sites (PEX) (Figure 3A, Supplemental Figure 5A, and Supplemental Table 3), and based sequence design on thermophysical properties (GC content between 40% and 60%, avoidance of C or G stretches, absence of self-hybridization) (51, 52). We first

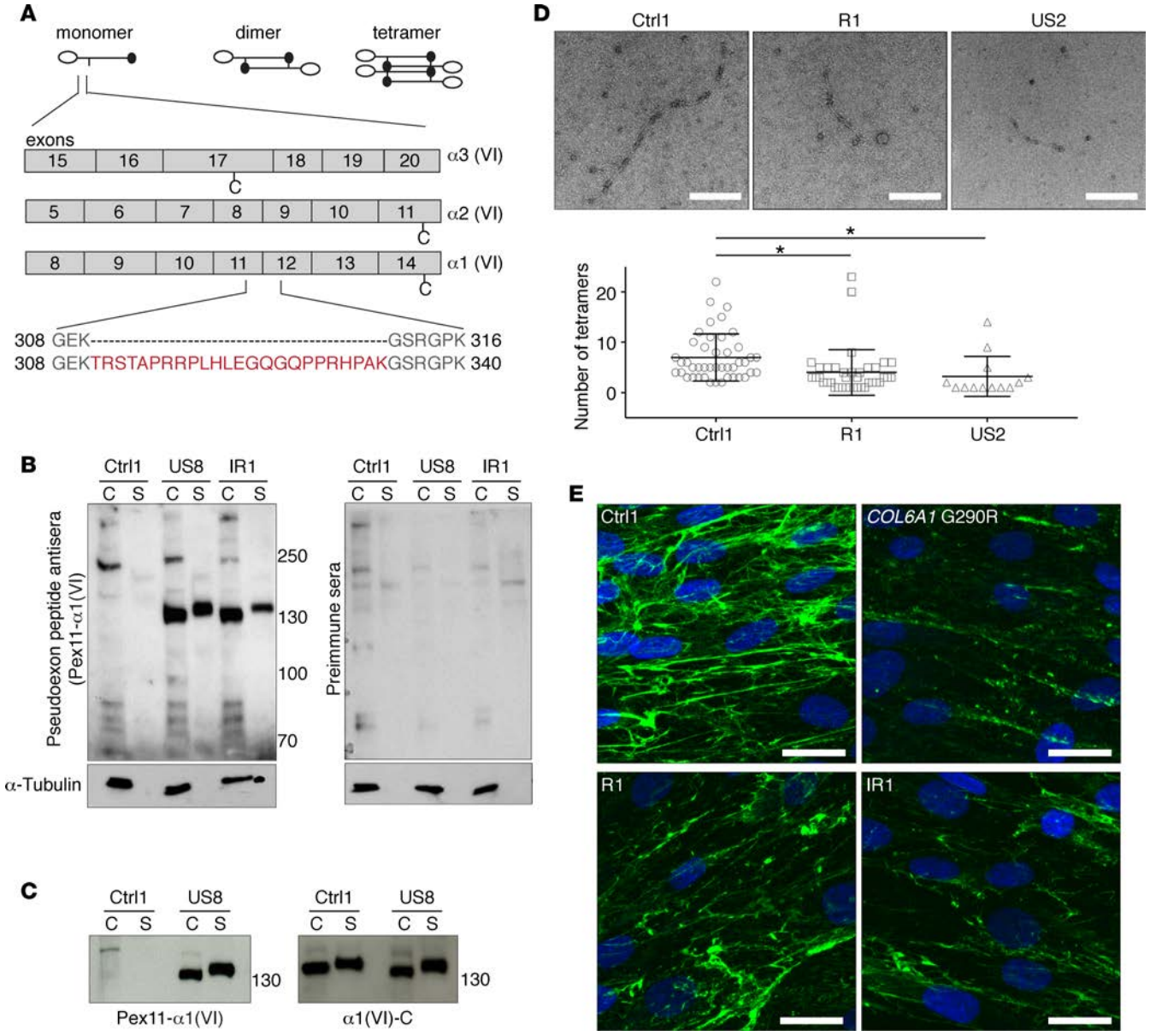

Figure 2. The *COL6A1* pseudoexon is translated and exerts a dominant-negative effect on collagen VI matrix assembly in cultured dermal fibroblasts. (**A**) Schematic representing the exon composition of the triple helical domains' N-terminal ends for each of the 3 α chains of collagen VI, including the predicted pseudoexon peptide sequence (shown in red) inserted between exons 11 and 12 of the α1 chain. The positions of the cysteine residues critical for dimer and tetramer stabilization are indicated for each chain. (**B**) A polyclonal antibody [Pex11-α1(VI)] was raised against the pseudoexon peptide, and used to probe a denaturing and reducing immunoblot of cell lysate (cellular, C) and media (secreted, S) protein extracts from cultured dermal fibroblasts of 2 patients and 1 unaffected individual. Probing with the preimmune sera is shown (right). (**C**) An immunoblot prepared as described in **B** was probed with the Pex11-α1(VI) antibody (left), then stripped and probed with an antibody detecting α1(VI) collagen [α1(VI)-C] (right). (**D**) Dermal fibroblasts were cultured in the presence of L-ascorbic acid, and medium was collected to measure collagen VI microfibrillar length using rotary shadowing electron microscopy (EM). Representative negative-staining EM images showing isolated collagen VI microfibrils (13 to 44 microfibrils were imaged per sample). Scale bars: 200 nm. The collagen VI microfibrillar length (number of tetramers per microfibril) is reported as a dot plot (below), where lines represent mean ± standard deviation. $^*P < 0.001$ by Mann-Whitney *U* test, Bonferroni corrected for 2 comparisons. (**E**) Dermal fibroblasts from 1 unaffected individual, 1 patient carrying the glycine substitution *COL6A1* G290R, and 2 +189C>T patients were cultured for 3 days in the presence of L-ascorbic acid, and then cells were fixed and immunostained for matrix-deposited collagen VI (green) and with the nuclear stain DAPI (blue). Scale bars: 25 μm.

screened the series of oligomers in the mutant pET-Ex-11-13–expressing HEK293T cells, and used as an assessment the ratio of expression of the pseudoexon-included over the WT products. Pseudoexon/WT ratios decreased with increasing oligomer concentration, for all PMO and 2′OMe oligomer treatments, with the exceptions of 2′OMe-SD1 and 2′OMe-SD2 for which ratios remained stable (Figure 3B and Supplemental Figure 5B). Of the 4 PEX-targeting PMOs (PMO-PEX1 to -PEX4), PMO-PEX1 and -PEX2 low-

Table 1. Detection of the collagen α1(VI) pseudoexon peptide in cultured dermal fibroblasts with liquid chromatography–tandem mass spectrometry

Enzyme	Dermal fibroblast ID	Fraction	Mascot score of α1 type VI collagen	Pseudoexon detection	
				Peptide sequence	Peptide *m/z* value
Trypsin	Ctrl1	Cellular	2,095	N/A	N/A
		Secreted	1,486	N/A	N/A
	US8	Cellular	1,494	RPLHLEGQGQPPR	495.61 (*z* = 3) 742.91 (*z* = 2)
		Secreted	1,308	RPLHLEGQGQPPR	742.91 (*z* = 2)
Chymotrypsin	Ctrl1	Cellular	1,283	N/A	N/A
		Secreted	918	N/A	N/A
	US8	Cellular	949	HLEGQGQPPRHPA	475.24 (*z* = 3) 712.36 (*z* = 2)
		Secreted	1,095	N/A	N/A

ered pseudoexon/WT ratios with superior efficacy (Figure 3B). Because the PMOs tested showed activity with this splicing reporter, and because the PMO chemistry has an excellent safety profile and is currently in several phase 3 clinical trials, we selected PMO-SA, -SD, -PEX1, and -PEX2 for the following experiments.

To test antisense oligomers in the context of their endogenous target, we treated 3 patient-derived dermal fibroblast lines, and used endpoint and quantitative RT-PCR assays to measure the relative levels of pseudoexon expression. Single treatments with the selected PMOs successfully suppressed pseudoexon inclusion in a dose-dependent manner (from 2.5 to 30 μM, Figure 3C). At the highest concentration tested, PMO-SA, -PEX1, -PEX2, and -SD suppressed relative pseudoexon levels down to 0.54, 0.136, 0.157, and 0.426, respectively, compared with nontargeting-treated (PMO-NT–treated) cells (relative expression of 0.971, Figure 3D). Remarkably, among the series of PMOs that we tested, those targeting PEX sequences were more effective than those directly targeting the mutant SD site. Similar superior effectiveness of targeting exonic splicing enhancer sites, or sites closer to the SA, as opposed to the splice sites, has been reported in other exon-skipping studies (discussed in ref. 52). This could indicate either that the mutant SD target sequence is difficult to access for the antisense oligomers because of the pre-mRNA tertiary structure and/or that binding of splicing enhancer factors at the pseudoexon site greatly contribute to its inclusion. In parallel, we measured total *COL6A1* expression levels by quantitative RT-PCR, and found that they remained stable (Figure 3E), which was consistent with redirection of splicing being the main mechanism for pseudoexon suppression, rather than mRNA knockdown.

We assessed whether combining nonoverlapping antisense oligomers into a single treatment could increase pseudoexon-skipping efficiency. We tested the 2 most effective compounds, PMO-PEX1 and PMO-PEX2, each in combination with PMO-SD. Treating cells with either combination skipped the pseudoexon with only slightly higher efficiency than each PMO separately at the comparative individual concentration (Figure 3F). For example, at 15 μM, treatment with PMO-PEX2 or with PMO-SD reduced pseudoexon expression levels down to 0.172 and 0.569, respectively. When combined in a single treatment of 30 μM total, PMO-PEX2 and PMO-SD reduced pseudoexon levels to 0.116, comparable to a single treatment with PMO-PEX2 at 30 μM.

Next, we sought to determine whether pseudoexon skipping, mediated either by PMO-PEX1 alone or by a combination of PMO-PEX2 and PMO-SD, correlated with reduced expression of the mutant-pseudoexon-containing collagen α1(VI) chain and with improved matrix deposition. We collected medium (secreted) and cell lysate (cellular) fractions from patients' fibroblasts treated with PMOs, and proceeded to immunoblotting using either a collagen α1(VI) antibody or the pseudoexon-specific antibody. We observed a marked decrease of the mutant protein expression together with stable total collagen α1(VI) levels following either treatment, in both the cellular and the secreted fractions (Figure 4A). Furthermore, we found that these PMO treatments improved collagen VI matrix morphology in culture, by increasing the deposition of thicker, longer, and continuous microfibrils, in 3 cell lines tested, as observed by immunofluorescence (Figure 4B). Consistent with these observations, using negative-staining electron microscopy, we found that treatment with the PMO-PEX2 and PMO-SD combination significantly increased collagen VI continuous microfibrillar length in one patient cell line (R1), resulting in a higher number of tetramers per microfibrils in the oligomer-treated compared with the nontargeting-PMO-treated and

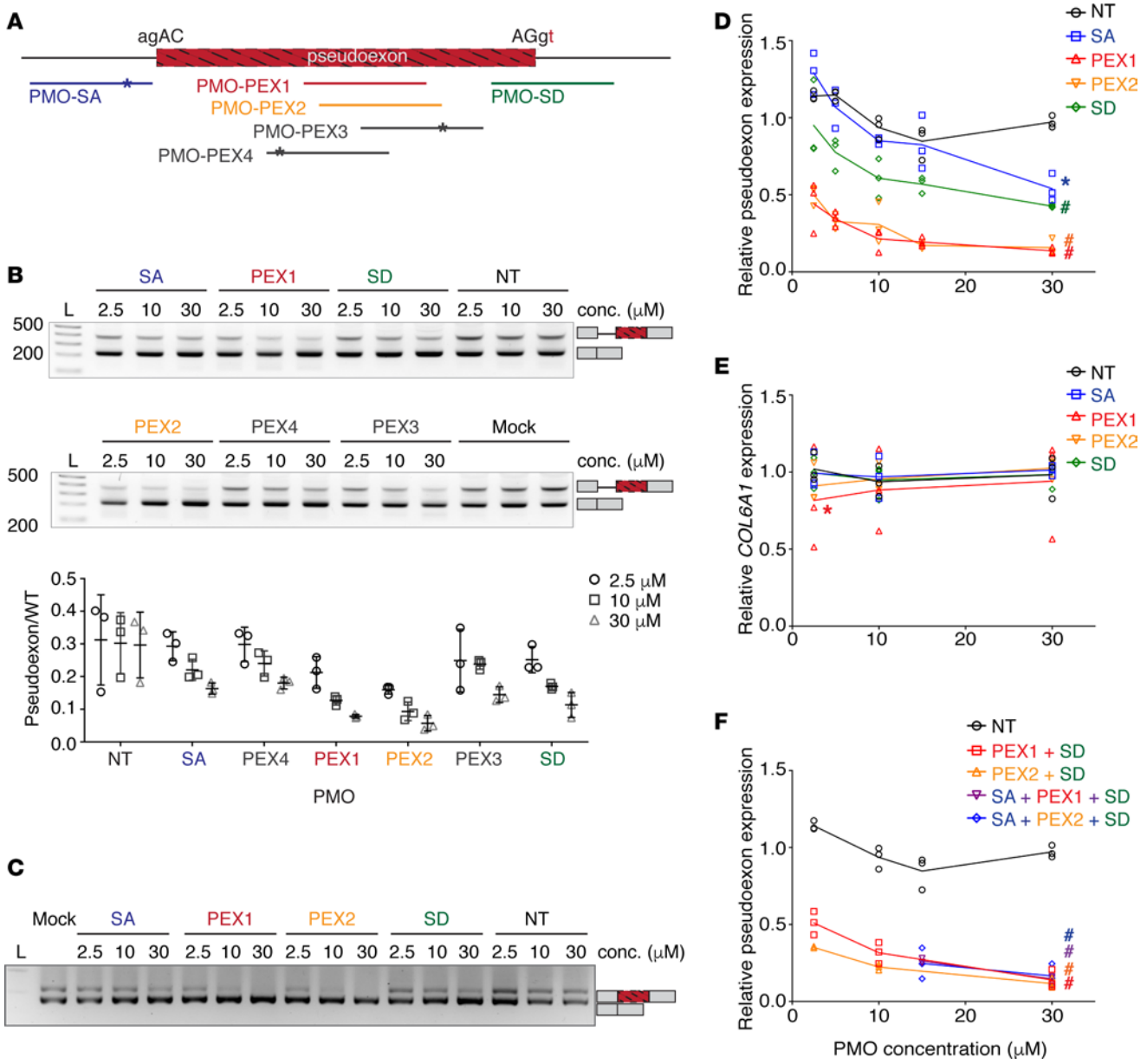

Figure 3. PMOs efficiently skip the *COL6A1* pseudoexon. (**A**) Location of the phosphorodiamidate morpholino antisense oligomers (PMOs) targeting the splice acceptor (SA), the splice donor (SD), or sequences within the pseudoexon (PEX). Asterisks in PMO-SA, PMO-PEX3, and PMO-PEX4 denote the presence of a mismatch between the oligomer sequence and the target sequence. (**B**) HEK293T cells expressing the minigene construct Ex-11-13 were transfected with each PMO oligomer at the indicated concentrations, and RNA was isolated 48 hours later. Electrophoretic gels of RT-PCR products amplified as in Figure 1E are shown (top), representative of 3 transfection replicates. PCR fragment densities were quantified from the gel images using ImageJ, to determine the ratio of pseudoexon over normal (pseudoexon/WT) products for each lane. Graph (bottom) reports the pseudoexon/WT ratios from 3 replicate treatments. Lines represent the average of the technical replicates ± standard deviation. PMO-NT = nontargeting PMO. Mock = transfection reagent only. (**C**) RT-PCR detection of the pseudoexon expression in patient IR1 cultured dermal fibroblasts following a 48-hour treatment with selected PMOs is shown as an example. (**D**–**F**) Relative gene expression in patient-derived cultured dermal fibroblasts treated for 48 hours with PMOs at the indicated concentrations, measured by quantitative RT-PCR assays specific for the pseudoexon (**D** and **F**) or for total *COL6A1* (**E**). Expression levels were normalized to the housekeeping gene *PGK1* and measured as relative to the corresponding mock-treated fibroblasts. Each data point represents the average of 2 to 3 treatments on 1 biological replicate, and lines represent the average of the 3 biological replicates (patients R1, IR1, and CA1). Repeated-measures 2-way ANOVA with Bonferroni's multiple comparisons test was applied. #$P < 0.05$ for all concentrations on the graph; *$P < 0.05$ for the indicated concentration.

untreated samples (Figure 4C). Unexpectedly, PMO treatment also significantly increased collagen VI microfibrillar length in an unaffected control sample, although at a lower *P* value (Figure 4C). Altogether, these results demonstrate that the PMOs selected in this study are potent effectors of pseudoexon skipping, which in turn abrogates the pseudoexon load and improves collagen VI matrix morphology.

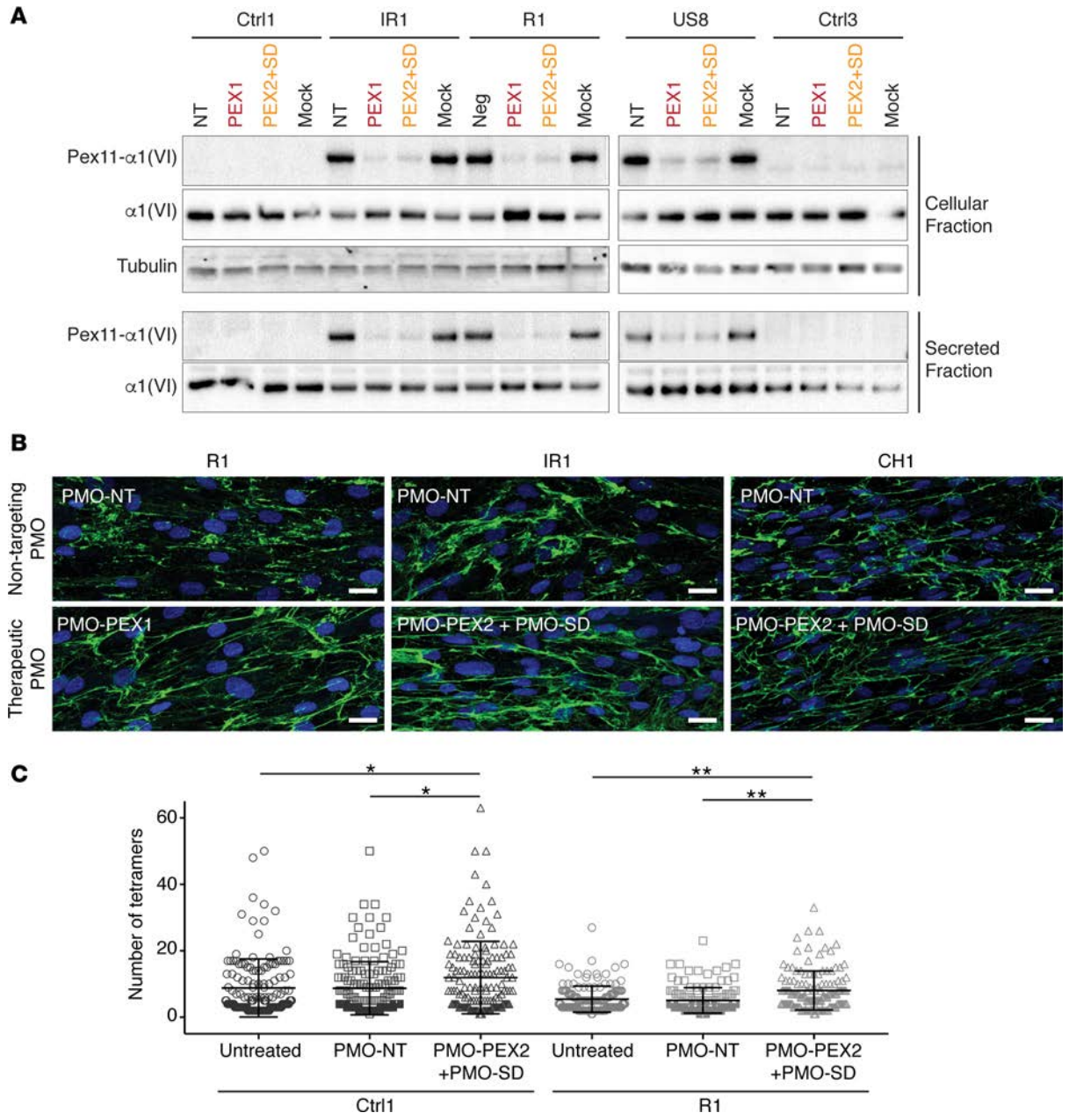

Figure 4. Skipping of the *COL6A1* pseudoexon mitigates the dominant-negative effect in cultured dermal fibroblasts. Cultured dermal fibroblasts from controls and patients were treated with the nontargeting control PMO (PMO-NT), or with PMO-PEX1, or a combination of PMO-PEX2 and PMO-SD, at a total PMO concentration of 30 μM for each condition, in the presence of L-ascorbic acid, for 4 days. (**A**) Immunoblots of the medium (secreted) or cell lysate (cellular) fractions were probed with the pseudoexon-specific antibody [Pex11-α1(VI)], and then blots were stripped and probed with an antibody detecting collagen α1(VI). Tubulin was probed as control. Mock = transfection reagent only. (**B**) Fibroblast cultures were fixed and stained for matrix-deposited collagen VI (green). Nuclei were stained with DAPI (blue). Scale bars: 25 μm. (**C**) Microfibrillar length (number of tetramers per collagen VI microfibril) was measured as described in Figure 2D, and is reported as a dot plot. Lines represent mean ± standard deviation. $^{*}P < 0.05$, $^{**}P < 0.0002$ by Mann-Whitney *U* test, Bonferroni corrected for 2 comparisons.

Correction of the COL6A1 pseudoexon mis-splicing using CRISPR/Cas9. We next devised a therapeutic strategy that could lead to permanent correction of the splice defect through gene editing. We used a dual-gRNA system to induce an intronic deletion encompassing the pseudoexon sequence along with the site of the mutation to restore normal expression from the mutant allele. This strategy would not be allele specific, but we surmised that because the cuts are deep in the intron (93 bp from exon 11 and 282 bp from exon 12) it would not affect processing of the intron allowing for normal splicing of both alleles. We designed a pair of gRNAs (annotated upstream 1 or U1, and downstream 1 or D1) flanking the pseudoexon sequence for

a predicted 103-bp deletion (Figure 5A). We first transfected into HEK293T cells a pSpCas9BB-2A-GFP dual-guide-expressing plasmid carrying both gRNAs, and enriched cells for GFP expression by fluorescence-activated flow cytometry, to validate dual-gRNA excision potential at the target region (Figure 5B). Next, we tested the efficacy of this dual-gRNA approach to skip the pseudoexon in the splicing reporter assay (Ex-10-13). Amplification of the minigene cDNA showed successful skipping of the splice-gain product from the +189T construct, and no change in expression from the +189C construct (Figure 5C).

Next, we nucleofected patient-derived fibroblasts with 10 μg of the pSpCas9BB-2A-GFP dual-guide plasmid, enriched cells for GFP expression, and on genomic DNA amplification detected a truncated fragment corresponding to 79.2% of total PCR products (43.5% when transfecting 5 μg of plasmid, Figure 5D), suggesting high efficiency of Cas9 cutting and DNA repair by excision. We quantified pseudoexon expression in the transfected IR1 fibroblasts by endpoint RT-PCR and found it to be reduced relative to fibroblasts transfected with the control plasmid (Figure 5E). The reduced pseudoexon expression again corresponded to a marked reduction of the mutant chain production (Figure 5F). Importantly, in control and in patient-derived transfected cells, total α1(VI) collagen production remained unchanged (Figure 5F), suggesting that the intronic deletion does not affect expression of the normal allele.

Discussion

Deep intronic variants that alter splicing are frequently inaccessible with exon-based diagnostic sequencing approaches. The recent incorporation of RNA sequencing and whole-genome sequencing into the diagnostic workflow for mutation-negative patients, however, has revealed such variants as an important class of disease-causing mutations (22). This is exemplified by our discovery of a de novo *COL6A1* deep intronic mutation (c.930+189C>T) (22), that we now report in a large cohort of 35 independent COL6-RD patients.

The discovery of this deep intronic *COL6A1* +189C>T mutation sheds light on a previously unrecognized mutational mechanism for COL6-RD: in-frame pseudoexonic insertion. In our cohort of 35 unrelated COL6-RD patients, we found this mechanism to be associated with an invariably severe UCMD phenotype, albeit with a seemingly delayed clinical presentation of symptoms compared with typical UCMD (1, 5, 18). The reasons for this delay and subsequent accelerated progression of symptoms in patients with this *COL6A1* +189C>T mutation are not yet clear and may be directly related to this particular *COL6* mutational mechanism, either due to (a) incomplete penetrance of the pseudoexon splice sites (mutant splice donor and cryptic splice acceptor), which causes the pseudoexon-inserted transcripts to be diluted out, and could be subject to temporal regulation; or (b) build-up of a dominant-negative, or toxic, mode of action carried out by the mutant-peptide-containing α1 chain; or both. An important consideration is that the pseudoexon encodes a noncollagenous peptide with potentially unique disruptive properties that is located at the N-terminal end of the triple helical domain, beyond the cysteine residue crucial for dimer stabilization, a location that enables the classical dominantly acting mutations mentioned above to be carried forward into the higher-order molecular structures of collagen VI. In this study, we provide evidence using mass spectrometry and immunoblotting with an antibody specific for the pseudoexon that the pseudoexon-containing α1(VI) chain is translated and secreted. Immunoblotting with an α1(VI) collagen antibody suggested that posttranslational processing of the α1(VI) chains (containing the pseudoexon or not) was seemingly similar. By immunofluorescence, however, we showed that the pseudoexon interferes with collagen VI matrix formation in culture, and leads to collagen VI mislocalization in muscle tissue. Intriguingly, interference with matrix formation is observed even when relatively low levels of the pseudoexon are spliced in, as is seen in dermal fibroblast cultures. One explanation is that the dominant-negative effect of the mutant α1 chain containing the pseudoexon peptide is amplified by its incorporation into the high-molecular-order collagen VI matrix assembly. The hampered end-to-end association of tetramers into beaded microfibrils and the irregular matrix formation we observed are consistent with such a mechanism. Moreover, the pseudoexon encodes a peptide sequence rich with positively charged residues (7 of 24) and likely adopts a misfolded structure interrupting the collagenous triple helical domain that could potentially not only inactivate tetramers but also initiate pathological and/or toxic interactions with other components in the matrix.

The discovery of the *COL6A1* +189C>T mutation immediately presented the opportunity to use rationally designed antisense therapies to promote exon skipping (or pseudoexon skipping) of this aberrant splice event, as potential interventions in COL6-RD patients carrying this mutation. The most promising option currently is the application of splice-modulating antisense oligomers. Successful advances in this technology are exemplified by the approval of 2 splice-modulating drugs by the FDA in the past 2

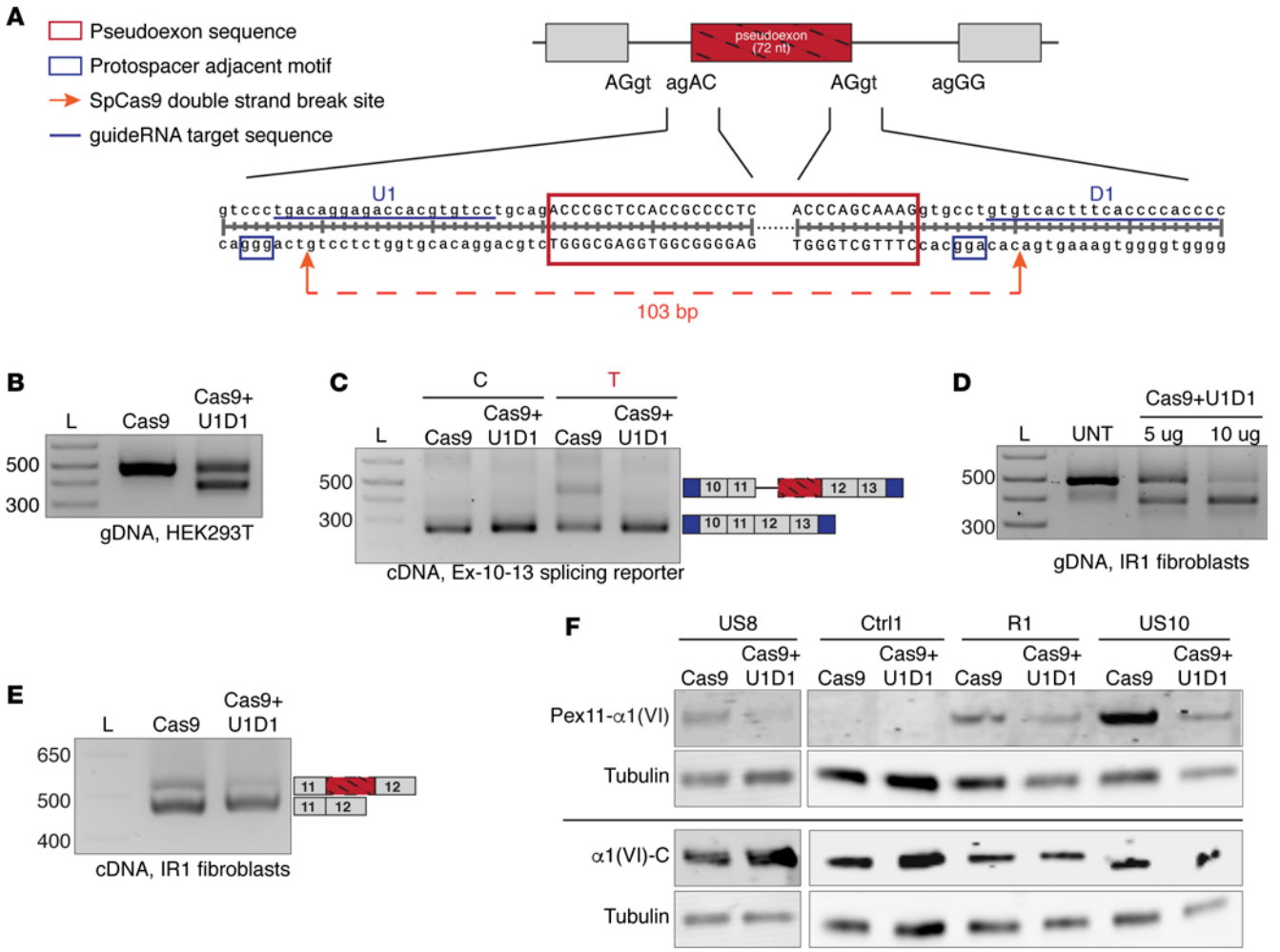

Figure 5. Cas9/dual-gRNA targeted genomic excision of the +189C>T mutation corrects the *COL6A1* pseudoexon splicing defect. (**A**) Schematic depicting position of the 2 gRNAs (gRNA upstream 1, U1; and downstream 1, D1) that were designed to excise a 103-nucleotide fragment harboring the pseudoexon-generating mutation from the deep intronic region of *COL6A1* intron 11. gRNA-U1 and -D1 were subcloned into a Cas9-GFP plasmid (Cas9+U1D1) harboring 2 gRNA cassettes for dual gRNA expression. (**B**) Amplification of genomic DNA from HEK293T cells transfected with 5 μg of the Cas9+U1D1 plasmid and GFP-enriched by cell sorting 48 hours after transfection. (**C**) HEK293T cells cotransfected with 1 μg of each splicing reporter (+189C, WT; +189T, mutant), and 5 μg of the Cas9+U1D1 plasmid, and sorted after 48 hours to enrich for GFP expression, were assessed for pseudoexon splicing by RT-PCR. (**D**) Amplification of genomic DNA from human patient fibroblast cell line IR1, 48 hours after nucleofection with 5 or 10 μg of the Cas9+U1D1 plasmid (GFP-sorted). (**E**) IR1 patient fibroblasts were nucleofected with 10 μg of Cas9+U1D1 plasmid, and sorted for GFP expression after 48 hours, before RNA isolation. Expression of the pseudoexon was assessed by endpoint RT-PCR. (**F**) US8 patient fibroblasts were nucleofected with 10 μg of Cas9+U1D1, followed by GFP enrichment, and cell lysates were harvested for immunoblotting. Membranes were probed with a pseudoexon-specific antibody [Pex11α1(VI)] and a housekeeping control (α-tubulin), or with an antibody assaying total collagen α1 (VI) expression [α1(VI)-C] and α-tubulin.

years (33, 36), including one designed to skip exon 51 of the *DMD* gene, as the first FDA-approved drug indicated for Duchenne muscular dystrophy, which has set a precedent for a regulatory pathway for this class of drugs. In contrast to Duchenne muscular dystrophy, in which the exon-skipping strategy is used to convert severe out-of-frame transcripts into in-frame and partially functional transcripts (similar to the internal deletion of alleles that results in the milder Becker muscular dystrophy), the pseudoexon-skipping approach explored here should have an even greater molecular benefit, as each event of successful skipping will generate a normal *COL6A1* mRNA. Similar to what has been observed when specifically knocking down dominant *COL6* mutations with the goal of converting to haploinsufficiency (53–56), suppressing the dominant-negative pseudoexon correlated with improved collagen VI matrix properties. For example, treatment with a combination of 2 PMO oligomers (PMO-PEX2 and PMO-SD) correlated with a marked reduction in detection of the mutant chain by the Pex11-α1(VI) antibody, improved collagen VI microfibril morphology, and increased collagen VI microfibrillar length. These results suggest that despite what must be a strong dominant-negative effect of this particular mutation, reducing its

expression improves matrix structure and has the potential to rescue collagen VI function. Our previously published observation of a substantial amelioration of clinical severity in patients with somatic mosaicism for other, typically severe, dominantly acting *COL6* mutations supports this assumption, as in such patients the dominant mutation load is diminished by virtue of the mosaicism (57).

Antisense oligomers would require lifelong repeat infusions to maintain activity. In contrast, gene editing would provide the potential for permanent correction after a single administration via a variety of possible in vivo delivery options. Here, we employed a dual-gRNA system to excise the pseudoexon sequence and were able to achieve a high excision efficiency in patient fibroblasts (up to 79.2%). This correlated with reduction of the pseudoexon inclusion and significant reduction of resulting mutant collagen α1(VI) chain. Even though the deep intronic excision approach does not discriminate between the WT and mutant alleles, it does not affect the expression and normal splicing from the WT allele, as determined by the total collagen VI α1 levels detected through immunoblotting in the control as well as in the patient cell lines treated with Cas9 and dual gRNAs. Translating this approach to the clinic is attractive, as the collagen VI–producing muscle interstitial cells are proliferative, meaning that genomic corrections would be transmitted to the cell progeny. Also, considering that collagen VI is a secreted protein that can extend into the extracellular space further away from its site of production, this mitigates the need for correction of all fibroblasts. While each of these 2 therapeutic strategies (antisense-mediated skipping and gene editing) possesses their advantages and disadvantages, the oligomer approach will be translatable to the clinic earlier, given the favorable safety profile of this approach. A conceivable therapeutic option in the future could be to first treat patients with a gene-editing approach and subsequently supplement with lower doses of oligomers in order to maximize any therapeutic effect by targeting alleles that may have escaped genomic correction. As the field of CRISPR research investigates potentially safer and more effective technologies for clinical translation, a promising approach our lab is currently pursuing is DNA base editing of the +189C>T mutation to restore normal splicing in the defective allele, with no double-stranded breaks and a template-free approach to achieve precise single-nucleotide mutations with a single gRNA (58).

Important questions remain to be addressed on the path to clinical translation. For instance, it is unclear whether a therapeutic oligomer can reach its target interstitial cell in diseased and potentially fibrotic muscles, and if so, whether reducing the mutational load could promote extracellular matrix remodeling after an abnormal matrix is already established, and finally, whether such remodeling could slow or reverse a decline in muscle function. In order to help answer these questions, an animal model is needed. The lack of homology between the human *COL6A1* intron 11 and the corresponding mouse *Col6a1* intron 11 precludes the mere introduction of the mutation in the mouse, a situation that could be circumvented by humanizing the relevant part of the *Col6a1* locus. Such a preclinical model would allow the targeting, skipping efficiency, and biological effect of human-ready antisense oligomers to be assessed in vivo, while also providing insights into the molecular pathogenesis as a consequence of this mutation.

In conclusion, we show that the identification of an unexpectedly common pseudoexon-activating deep intronic mutation by advanced next-generation sequencing–based technologies directly resulted in the development of rationally targeted therapeutic strategies. This, together with the even stronger rationale for dominant pseudoexon-inducing mutations such as the *COL6A1* +189C>T mutation and the in-patient cell efficacy data shown here, supports the feasibility of an accelerated translational path. In a broader context we have shown that combining RNA sequencing and whole-genome sequencing as diagnostic tools allows splice-altering mutations to be discovered at a surprisingly high frequency in previously undiagnosed patients (22). Many of these mutations would be amenable to a precision therapeutic strategy using individualized splice-modulating approaches. Our experience thus argues for wider use of these diagnostic tools and the development of a toolbox of class-approved therapeutic reagents that can be used to treat splice mutations rapidly, even at the single-patient level.

Methods

Human subjects. Subjects were recruited at the NIH through the Pediatric Neuromuscular Clinic (12-N-0095 approved by the Institutional Review Board of the National Institute of Neurological Disorders and Stroke [NINDS], NIH). Subjects were also identified through their local medical centers in Canada, Chile, Germany, Ireland, Latvia, Romania, UK, France, Italy, Australia, Spain, and Israel. Complete clinical assessment was performed by trained clinicians. Peripheral blood, skin biopsies, and muscle biopsy samples were obtained based on standard procedures.

Diagnostic work-up and genetic testing. Diagnostic work-up included histological and immunofluorescence staining of muscle biopsy sections, assessment of collagen VI matrix deposition by cultured dermal fibroblasts, and cDNA sequencing of the triple helical domains for the 3 main collagen VI genes (*COL6A1*, *COL6A2*, and *COL6A3*). Genomic DNA isolated from peripheral blood was used to screen for the *COL6A1* +189C>T mutation by targeted amplification and sequencing (with primers listed in Supplemental Table 4). PCR products were sent to Genewiz for Sanger sequencing.

RNA sequencing and PSI. RNA sequencing of muscle RNA from 4 patients (UK1, UK2, US1, and US2) was described in Cummings et al. (22). To compare the rate of inclusion of the intronic splice event in *COL6A1* in muscle and fibroblasts, we performed paired-end 76-bp sequencing on Illumina HiSeq 2000 instruments, with 50M sequence coverage for an RNA sample isolated from cultured skin fibroblasts (UK1). RNA sequencing data were aligned using Star 2-Pass version v.2.4.2a using hg19 as the genome reference and Gencode V19 annotations. We obtained inclusion of values for the intronic splice-gain event in samples as described in Schafer et al. (50).

Cloning. Cloning for dual gRNAs was performed in a dual-guide expression pDG458 plasmid (pDG458 was a gift from Paul Thomas, University of Adelaide, Adelaide, Australia; Addgene plasmid 100900). The selected gRNA sequences U1 and D1 were subcloned into the plasmid according to a pDG 1-step cloning protocol (59). Briefly, the guide sequences for upstream and downstream gRNA sequences were phosphorylated and annealed by mixing 100 pmol of each pair and 0.5 μl T4 PNK (NEB) and then incubated at 37°C for 30 minutes, followed by 95°C for 5 minutes, and slowly ramped to room temperature. Annealed oligos were diluted 1:125. Pairs of oligo duplexes were ligated into empty vectors in a 1-step digestion ligation reaction described previously (59). Plasmid DNA was isolated using an endotoxin-free maxiprep kit (Qiagen) and correct insertion of oligonucleotide duplexes into the vectors was confirmed using the sequencing primers U6 and BGH PA F (Supplemental Table 4). The upstream and downstream gRNA sequences were scored and selected using crispr.mit.edu. The sequences of the oligonucleotides used for cloning into the dual gRNA expressing SpCas9 plasmid are listed in Supplemental Table 4.

For additional cloning methods, see supplemental material.

Antisense oligomers. PMOs were designed following previously published guidelines (52) (Supplemental Table 3), and were purchased from GeneTools, LLC. For PMO-PEX3 and PMO-PEX4, mispairs (lower cases in the sequence) were voluntary introduced to reduce the G content and self-complementarity (Supplemental Table 3). PMOs were reconstituted to a 1 mM stock solution in water.

2′OMe antisense oligomers were synthesized at Murdoch University, using phosphorothioate bonds and 2′OMe-modified RNA analogs (Supplemental Table 3). In 2′OMe-PEX2, one mismatch was introduced (indicated in lower case, Supplemental Table 3).

Cell culture, transfection, nucleofection of Cas9 plasmids, and oligomer treatment. Dermal fibroblasts from normal controls and patients were established from skin biopsies. HEK293T cells were obtained from ATCC. All cell lines were routinely maintained in Dulbecco's modified Eagle medium (Gibco/ThermoFisher Scientific) supplemented with 10% fetal bovine serum (FBS) (Corning/ThermoFisher Scientific) and 1% penicillin/streptomycin (Gibco/ThermoFisher Scientific) at 37°C in 5% CO_2. At revival, cells were tested for mycoplasma contamination (MycoAlert mycoplasma detection kit, Lonza), and treated with MycoZap Reagent (Lonza) if found positive. Experiments were conducted on mycoplasma-negative cells.

Minigene plasmids (0.2 μg) were complexed with 1.5 μl of Lipofectamine 2000 or 3000 (Invitrogen/ThermoFisher Scientific) in OptiMEM (Invitrogen/ThermoFisher Scientific) and transfected into HEK293T cells in 500 μl of DMEM supplemented with 10% FBS, in 24-well plates. Cells were then incubated for 24 hours before RNA isolation.

Antisense oligomer treatments were carried out in 24-well plates. Patient-derived skin fibroblasts (3×10^4 cells) were seeded in each well. The next day, cells were washed once with DMEM, then fresh medium (either 300 μl of DMEM supplemented with 10% FBS for PMO transfection, or 200 μl of DMEM for 2′OMe oligomer transfection) was added to each well. For PMOs, the oligomer solutions were added to each well according to the desired final concentration, and the plate was gently swirled after each oligomer addition. Then, 2.6 μl of Endo-Porter (GeneTools) was added directly to each well, and the plate was vigorously swirled after each addition. Cells were incubated for 48 hours before RNA isolation. For 2′OMe oligomers, the oligomers were complexed with 1.5 μl of Oligofectamine (Invitro-

gen/ThermoFisher Scientific) in OptiMEM according to the desired final concentration, and 50 μl of the complex was added to each well. Five hours later, 125 μl of DMEM supplemented with 30% FBS was added to each well. Cells were incubated for 48 hours before RNA isolation.

For the antisense oligomer screen with the minigene system, HEK293T cells were incubated for 6 hours with the minigene DNA transfection mix. Cells were then washed once with DMEM, and the oligomer transfection was performed as described above. Cells were incubated for 48 hours before RNA isolation.

To determine Cas9 cutting efficiency, 1×10^5 of HEK293T cells were plated overnight into 6-well plates and the following day, 5 μg of Cas9 or Cas9+U1D1 was transfected using Lipofectamine 2000 (Invitrogen/ThermoFisher Scientific). Forty-eight hours after transfection, GFP enrichment was performed to harvest 2×10^5 cells that were processed for genomic DNA analysis. For the CRISPR/Cas9 experiments with minigene reporter assays, 5 μg of plasmid, either Cas9 only or Cas9+U1D1, was cotransfected with 1 μg of the minigene splicing reporter constructs. Forty-eight hours after transfection, cells were harvested in TRIzol (Ambion/ThermoFisher Scientific) for RNA isolation and RT-PCR analyses. Nucleofection of patient dermal fibroblast cells was performed as follows: 2×10^6 cells were diluted in P2 buffer (Lonza), mixed with either 5 μg or 10 μg of Cas9- or Cas9+U1D1–expressing plasmids, transferred to a cuvette, and subjected to the nucleofection program DT-130 (Lonza Amaxa 4D-nucleofector). After nucleofection, cells were allowed to sit for 10 minutes in the cuvette before pipetting the cells into 6-well plates for recovery. Forty-eight hours after nucleofection, cells were GFP-enriched and 1×10^5 cells were harvested for downstream analyses such as genomic DNA extraction, RNA extraction, and Western blotting.

RNA isolation and RT. Total RNA was isolated from muscle biopsy sections, or PBS-washed adherent cultured cells, using TRIzol. RNA (250 ng to 1 μg) was treated with 1 U of rDNase I using the DNA-free kit (Ambion/ThermoFisher Scientific). cDNA was synthesized with SuperScript III Reverse Transcriptase (Invitrogen/ThermoFisher Scientific), using the vector-specific primer 5′-ACTGATCCACGATGC-3′ (for minigene-transfected cell samples), or random primers (Invitrogen/ThermoFisher Scientific). For minigene-transfected samples, cDNA was quantified with Quant-iT Oligreen ssDNA (Invitrogen/ThermoFisher Scientific) and diluted to 5 ng/μl before amplification.

Quantitative PCR amplification. The quantitative PCR (qPCR) primer/probe mix to detect pseudoexon-included transcripts was purchased as a PrimeTime qPCR Assay (Integrated DNA Technologies; Supplemental Table 4). To measure total *COL6A1* expression or the endogenous control gene phosphoglycerate kinase 1 (*PGK1*, Supplemental Table 4), the hydrolysis probes were purchased from the Universal Probe Library (UPL, Roche Applied Science). qPCR reactions were performed in a total volume of 10 μl, with 3 μl of cDNA and a 1× final concentration of the FastStart Master mix (containing ROX) (Roche Applied Science). The PrimeTime primers/probe mix was used at a 1× final concentration, while the UPL probe was used at 0.4 μM, with primers at 0.7 μM each. qPCR reactions were run in quadruplicate, at 50°C for 2 minutes, 95°C for 10 minutes, followed by 40 cycles of 95°C for 15 seconds and 60°C for 1 minute, on the QuantStudio 6 Flex Real-Time PCR System (Applied Biosystems/ThermoFisher Scientific). Ct values were determined by the QuantStudio Real-Time PCR software (Applied Biosystems/ThermoFisher Scientific). The comparative Ct (ΔΔCt) method was applied to measure the relative expression, using the *PGK1* Ct values as the endogenous normalizing gene, and the ΔCt values from the untreated controls as the normalizing value.

Methods for routine PCR and sequencing can be found in supplemental material.

Matrix immunofluorescence. Patient-derived skin fibroblasts were seeded (1.5×10^4 cells per well) in 8-chamber tissue culture slides (Corning/ThermoFisher Scientific). The next day, medium was replaced with complete medium, supplemented with 50 μg/ml of L-ascorbic acid (Wako Chemicals). Two days later, medium was replaced to provide a fresh supply of L-ascorbic acid. The following day (3 days of L-ascorbic acid treatment), cells were washed in PBS once, then fixed in 4% paraformaldehyde (Electron Microscopy Sciences) for 10 minutes at room temperature. For antisense oligomer treatment followed by matrix staining, the same procedure was applied with these modifications: 0.7×10^4 cells per well were seeded, medium was replaced the next day to supplement with antisense oligomers (as described above), 2 days later medium was replenished with fresh supply of antisense oligomers and L-ascorbic acid, 2 days later fresh L-ascorbic acid was added to the wells, and cells were fixed 3 days after L-ascorbic acid treatment (5 days after oligomer treatment).

For staining, cells were washed in PBS, then blocked for 1 hour with 10% FBS in PBS, with or without 0.1% Triton X-100 (MilliporeSigma). Primary antibodies were diluted in the blocking buffer and applied to samples for 3 hours at room temperature. Samples were washed 3 times for 5 minutes with

PBS, and incubated with secondary antibodies, diluted in blocking buffer, for 1 hour at room temperature. Samples were again washed with PBS 3 times for 5 minutes each and incubated with 4′,6-diamidino-2-phenylindole, dihydrochloride (DAPI) diluted in PBS, for 15 minutes. Samples were washed with PBS twice, and mounted with Fluoromount-G (SouthernBiotech). Antibodies used were as follows: mouse anti–human collagen VI (MAB1944, clone 3C4, MilliporeSigma); rabbit anti-fibronectin (F3648, MilliporeSigma); goat anti-mouse IgG, Alexa Fluor 488 (A-11001, Invitrogen/ThermoFisher Scientific); and goat anti–rabbit IgG, Alexa Fluor 568 (A-11036, Invitrogen/ThermoFisher Scientific).

Confocal microscopy. Images were acquired on a TCS SP5 II system (Leica Microsystems), with ×40 or ×63 objectives. The pinhole was adjusted to obtain a section thickness of 0.508 μm, and *Z*-stacks were acquired using 0.5-μm-sized steps. Stacks were merged.

Pseudoexon-specific antibody. A polyclonal antibody was raised against the mutant peptide as follows. The peptide with sequence (TRSTAPRRPLHLEGQGQPPRHPAK-C) was synthesized (Pineda Antikörper-Service) and disulfide linked via the C-terminal cysteine to keyhole limpet hemocyanin (KLH). The conjugate was used for immunization of a rabbit and antibodies raised in the serum harvested at 60 days after injection.

Immunoblotting. Patient-derived skin fibroblasts were treated with antisense oligomers in 24-well plates as described above but were incubated for a total of 4 days in the presence of the oligomers. Twenty-four hours after the start of oligomer treatment, L-ascorbic acid was added to each well for a final concentration of 50 μg/ml. Four days after the start of oligomer treatment, medium was collected in a prechilled 1.5-ml tube, containing a final 1× concentration of Complete Protease Inhibitor cocktail (Roche Applied Science), then was spun for 10 minutes at 15,000 *g* at 4°C, and supernatant was collected. The cell layer was washed twice with cold PBS and lysed with RIPA buffer (50 mM Tris-HCl pH 8.0, 150 mM NaCl, 0.5% sodium deoxycholate, 0.1% SDS, 1% NP-40) containing 1× Complete Protease Inhibitor cocktail. Samples were incubated on ice for 30 minutes, then spun for 20 minutes at 15,000 *g* at 4°C, and supernatant was collected. Protein concentrations were determined using BCA protein assay (ThermoFisher Scientific). Protein samples were diluted in NuPAGE LDS Sample Buffer (final concentration 1×; ThermoFisher Scientific), with 5% 2-mercaptoethanol (MP Biomedicals), boiled for 5 minutes at 95°C, and vortexed. Denatured protein samples (5 μg for cell lysates [or cellular fraction], 15 μg for medium [or secreted fraction]) were loaded onto a NuPAGE 4%–12% Bis-Tris gel (ThermoFisher Scientific), and run with 1× NuPAGE MOPS SDS Running buffer (ThermoFisher Scientific) for 50 minutes at 200 V. Samples were transferred onto Immobilon-P PVDF membranes (MilliporeSigma) using 1× NuPAGE Transfer buffer containing 5% methanol, for 1.5 hours at 25 V. Membranes were blocked with 5% milk in TBS containing 0.05% Tween-20 (TBS-T) (MilliporeSigma). Membranes were incubated with primary antibodies diluted in blocking solution overnight at 4°C, followed by washing 3 times for 5 minutes each with TBS-T. Membranes were then incubated with secondary antibodies in blocking solution for 2 hours at room temperature, followed by 3 times for 5 minutes each with TBS-T. When using HRP-linked secondary antibodies, chemiluminescence was detected using a Clarity Western ECL kit (Bio-Rad), and imaged on the ChemiDoc XRS+ Imaging System (Bio-Rad). For fluorescently labeled secondary antibodies, membranes were imaged on the Odyssey CLx system (LI-COR Biosciences). The antibodies used were as follows: rabbit anti-pseudoexon (1:50 dilution); rabbit anti–collagen α1(VI) (1026, gift from Mon Li-Chu, Thomas Jefferson University, Philadelphia, USA; 1:7,500 dilution); mouse anti-tubulin, clone B-5-1-2 (T5168, MilliporeSigma, 1:6,000 dilution); anti–rabbit IgG, HRP-linked (Cell Signaling Technology, 1:1,000 dilution); anti–mouse IgG–HRP (PerkinElmer, 0.05 μg/ml); goat anti–rabbit IgG IRDye 680RD (LI-COR Biosciences, 1:1,000 dilution); and goat anti–mouse IgG IRDye 800CW (LI-COR Biosciences, 1:1,000 dilution).

Negative-staining electron microscopy. Patient-derived skin fibroblasts (2.5×10^4 cells) were plated in single wells of 12-well plates. When cells reached approximately 60% confluence, antisense oligomer treatments were performed as described above. After 48 hours, medium was removed, and a second oligomer treatment was performed in the presence of L-ascorbic acid, as described above. After 48 hours (4 days after start of oligomer treatment), cells were washed twice with PBS, and then incubated in a small volume (250 μl) of DMEM supplemented with L-ascorbic acid (serum-free medium) for 16 hours. Medium was collected and supplemented with complete protease inhibitor cocktail (Roche Applied Science, 1× final concentration) and sodium azide (0.1% final concentration). Samples were spun at 15,000 *g* for 10 minutes at 10°C, and supernatants were collected and stored at 4°C. Microfibrils were deposited on a carbon-coated electron microscopy grid, stained for 30 seconds with 1% aqueous uranyl acetate, blotted, and quickly air dried. Grids were observed at 300 kV using a Tecnai F30 (FEI) and micrographs were acquired with an Utrascan 1000 (Gatan). Grids were systematically scanned and 134–147 microfibrils were measured in each sample.

Statistics. To compare collagen VI microfibrillar length, statistical significance between groups was assessed using Mann-Whitney *U* test, followed by Bonferroni's correction for multiple comparisons. For the relative expression data (from the qPCR experiments), significance between groups was tested using repeated-measures 2-way ANOVA with Bonferroni's correction. *P* values of <0.05 were considered significant.

Study approval. This study was approved by the Institutional Review Board of the National Institute of Neurological Disorders and Stroke, NIH (12-N-0095). All subjects provided informed consent prior to participating in the study. Subjects were also identified through their local medical centers.

Author contributions

CGB, FM, DGM, VB, ARF, and A. Sarathy conceptualized and designed the study and the experiments. BBC, ML, TT, JLM, and DGM performed and analyzed the RNA sequencing study. ARF, SD, A. Sarkozy, JK, TS, SQR, EB, LM, GC, GY, EL, SMG, RR, JC, MS, MEL, CG, BDK, MT, BL, ANO, MMR, GJ, IN, RJB, CJM, FG, CG, AF, VA, CJ, and DMY recruited patients, collected patients' samples, and analyzed phenotypical data. CG, KM, and VA collected and performed the experiments on the muscle-derived fibroblasts. VB, SDW, OR, and HZ designed antisense oligomers. EH and SRL performed and analyzed the negative-staining electron microscopy experiments. HSD and RW developed and assayed the mutant peptide-specific antibody. YL conducted the mass spectrometry experiments and analyses. VB, YH, A. Sarathy, KS, MN, GSC, and SA performed all other experiments. VB, ARF, and CGB wrote the manuscript.

Acknowledgments

The authors thank Mon-Li Chu for providing the collagen VI antibody, Dragan Maric for sharing his expertise in fluorescence-activated cell sorting, and Gina Norato for reviewing the statistical analyses. This study was supported by National Institute of Neurological Disorders and Stroke intramural funds to CGB (1ZIANS003129-08), and by the German Research Council (CRC 829-B2, FOR 2722-B1) to RW. We acknowledge contributing funding and support from CureCMD and Muscular Dystrophy UK. VB is the recipient of a Canadian Institutes of Health Research Fellowship, a Fonds de Recherche Québec – Santé Fellowship, and of a Muscular Dystrophy Association Development Grant (MDA513460). FM is supported by the National Institute for Health Research Biomedical Research Centre at Great Ormond Street Hospital for Children NHS Foundation Trust and University College London. FM gratefully acknowledges the support of the Centre for Neuromuscular Disease Biobank, and of the Muscular Dystrophy UK. The views expressed are those of the author(s) and not necessarily those of the NHS, the NIHR or the Department of Health. CJM is funded by the Plan Nacional de I+D+ I and Instituto de Salud Carlos III Subdirección General de Evaluación y Fomento de la Investigación Sanitaria (projects PI16/ PI16/00579 and CP09/00011 to CJM), and the European Regional Development Fund (FEDER, A way to make Europe). CJM is indebted to the "Biobanc de l'Hospital Infantil Sant Joan de Déu per a la Investigació" integrated in the Spanish Biobank Network of ISCIII for the sample and data procurement. DGM was supported by the National Human Genome Research Institute, the National Eye Institute, and the National Heart, Lung and Blood Institute grant UM1 HG008900. See supplemental material for the *COL6A1* Intron 11 Study Group consortium details.

Address correspondence to: Carsten G. Bönnemann, National Institute of Neurological Disorders and Stroke/NIH, Porter Neuroscience Research Center, Building 35, Room 2A-116, 35 Convent Drive, Bethesda, Maryland 20892, USA. Phone: 1.301.594.5496. Email: carsten.bonnemann@nih.gov.

1. Bönnemann CG. The collagen VI-related myopathies: muscle meets its matrix. *Nat Rev Neurol*. 2011;7(7):379–390.
2. Okada M, et al. Primary collagen VI deficiency is the second most common congenital muscular dystrophy in Japan. *Neurology*. 2007;69(10):1035–1042.
3. Norwood FL, Harling C, Chinnery PF, Eagle M, Bushby K, Straub V. Prevalence of genetic muscle disease in Northern England: in-depth analysis of a muscle clinic population. *Brain*. 2009;132(Pt 11):3175–3186.
4. Clement EM, et al. Relative frequency of congenital muscular dystrophy subtypes: analysis of the UK diagnostic service 2001-2008. *Neuromuscul Disord*. 2012;22(6):522–527.
5. Nadeau A, et al. Natural history of Ullrich congenital muscular dystrophy. *Neurology*. 2009;73(1):25–31.
6. Foley AR, et al. Natural history of pulmonary function in collagen VI-related myopathies. *Brain*. 2013;136(Pt 12):3625–3633.
7. Zou Y, Zhang RZ, Sabatelli P, Chu ML, Bönnemann CG. Muscle interstitial fibroblasts are the main source of collagen VI synthesis in skeletal muscle: implications for congenital muscular dystrophy types Ullrich and Bethlem. *J Neuropathol Exp Neurol*. 2008;67(2):144–154.
8. Braghetta P, et al. An enhancer required for transcription of the Col6a1 gene in muscle connective tissue is induced by signals

released from muscle cells. *Exp Cell Res*. 2008;314(19):3508–3518.
9. Furthmayr H, Wiedemann H, Timpl R, Odermatt E, Engel J. Electron-microscopical approach to a structural model of intima collagen. *Biochem J*. 1983;211(2):303–311.
10. Engvall E, Hessle H, Klier G. Molecular assembly, secretion, and matrix deposition of type VI collagen. *J Cell Biol*. 1986;102(3):703–710.
11. Lamandé SR, et al. The role of the alpha3(VI) chain in collagen VI assembly. Expression of an alpha3(VI) chain lacking N-terminal modules N10-N7 restores collagen VI assembly, secretion, and matrix deposition in an alpha3(VI)-deficient cell line. *J Biol Chem*. 1998;273(13):7423–7430.
12. Baldock C, Sherratt MJ, Shuttleworth CA, Kielty CM. The supramolecular organization of collagen VI microfibrils. *J Mol Biol*. 2003;330(2):297–307.
13. Godwin ARF, Starborg T, Sherratt MJ, Roseman AM, Baldock C. Defining the hierarchical organisation of collagen VI microfibrils at nanometre to micrometre length scales. *Acta Biomater*. 2017;52:21–32.
14. Pan TC, Zhang RZ, Sudano DG, Marie SK, Bönnemann CG, Chu ML. New molecular mechanism for Ullrich congenital muscular dystrophy: a heterozygous in-frame deletion in the COL6A1 gene causes a severe phenotype. *Am J Hum Genet*. 2003;73(2):355–369.
15. Engel J, et al. Structure and macromolecular organization of type VI collagen. *Ann N Y Acad Sci*. 1985;460:25–37.
16. Baker NL, et al. Dominant collagen VI mutations are a common cause of Ullrich congenital muscular dystrophy. *Hum Mol Genet*. 2005;14(2):279–293.
17. Lampe AK, et al. Exon skipping mutations in collagen VI are common and are predictive for severity and inheritance. *Hum Mutat*. 2008;29(6):809–822.
18. Briñas L, et al. Early onset collagen VI myopathies: Genetic and clinical correlations. *Ann Neurol*. 2010;68(4):511–520.
19. Allamand V, Briñas L, Richard P, Stojkovic T, Quijano-Roy S, Bonne G. ColVI myopathies: where do we stand, where do we go? *Skelet Muscle*. 2011;1:30.
20. Butterfield RJ, et al. Position of glycine substitutions in the triple helix of COL6A1, COL6A2, and COL6A3 is correlated with severity and mode of inheritance in collagen VI myopathies. *Hum Mutat*. 2013;34(11):1558–1567.
21. Pace RA, et al. Collagen VI glycine mutations: perturbed assembly and a spectrum of clinical severity. *Ann Neurol*. 2008;64(3):294–303.
22. Cummings BB, et al. Improving genetic diagnosis in Mendelian disease with transcriptome sequencing. *Sci Transl Med*. 2017;9(386):eaal5209.
23. Rimessi P, et al. Antisense modulation of both exonic and intronic splicing motifs induces skipping of a DMD pseudo-exon responsible for X-linked dilated cardiomyopathy. *Hum Gene Ther*. 2010;21(9):1137–1146.
24. Blázquez L, et al. In vitro correction of a pseudoexon-generating deep intronic mutation in LGMD2A by antisense oligonucleotides and modified small nuclear RNAs. *Hum Mutat*. 2013;34(10):1387–1395.
25. Rendu J, et al. Exon skipping as a therapeutic strategy applied to an RYR1 mutation with pseudo-exon inclusion causing a severe core myopathy. *Hum Gene Ther*. 2013;24(7):702–713.
26. Dominov JA, et al. A novel dysferlin mutant pseudoexon bypassed with antisense oligonucleotides. *Ann Clin Transl Neurol*. 2014;1(9):703–720.
27. Palhais B, et al. Splice-shifting oligonucleotide (SSO) mediated blocking of an exonic splicing enhancer (ESE) created by the prevalent c.903+469T>C MTRR mutation corrects splicing and restores enzyme activity in patient cells. *Nucleic Acids Res*. 2015;43(9):4627–4639.
28. Garanto A, et al. In vitro and in vivo rescue of aberrant splicing in CEP290-associated LCA by antisense oligonucleotide delivery. *Hum Mol Genet*. 2016;25(12):2552–2563.
29. Slijkerman RW, et al. Antisense oligonucleotide-based splice correction for USH2A-associated retinal degeneration caused by a frequent deep-intronic mutation. *Mol Ther Nucleic Acids*. 2016;5(10):e381.
30. Heemskerk HA, et al. In vivo comparison of 2′-O-methyl phosphorothioate and morpholino antisense oligonucleotides for Duchenne muscular dystrophy exon skipping. *J Gene Med*. 2009;11(3):257–266.
31. Kole R, Krieg AM. Exon skipping therapy for Duchenne muscular dystrophy. *Adv Drug Deliv Rev*. 2015;87:104–107.
32. Douglas AG, Wood MJ. Splicing therapy for neuromuscular disease. *Mol Cell Neurosci*. 2013;56:169–185.
33. Aartsma-Rus A, Krieg AM. FDA approves eteplirsen for Duchenne muscular dystrophy: the next chapter in the eteplirsen saga. *Nucleic Acid Ther*. 2017;27(1):1–3.
34. Mendell JR, et al. Longitudinal effect of eteplirsen versus historical control on ambulation in Duchenne muscular dystrophy. *Ann Neurol*. 2016;79(2):257–271.
35. Finkel RS, et al. Nusinersen versus Sham control in infantile-onset spinal muscular atrophy. *N Engl J Med*. 2017;377(18):1723–1732.
36. Aartsma-Rus A. FDA approval of nusinersen for spinal muscular atrophy makes 2016 the year of splice modulating oligonucleotides. *Nucleic Acid Ther*. 2017;27(2):67–69.
37. Doudna JA, Charpentier E. Genome editing. The new frontier of genome engineering with CRISPR-Cas9. *Science*. 2014;346(6213):1258096.
38. Ousterout DG, Kabadi AM, Thakore PI, Majoros WH, Reddy TE, Gersbach CA. Multiplex CRISPR/Cas9-based genome editing for correction of dystrophin mutations that cause Duchenne muscular dystrophy. *Nat Commun*. 2015;6:6244.
39. Xu L, et al. CRISPR-mediated genome editing restores dystrophin expression and function in mdx mice. *Mol Ther*. 2016;24(3):564–569.
40. Long C, et al. Postnatal genome editing partially restores dystrophin expression in a mouse model of muscular dystrophy. *Science*. 2016;351(6271):400–403.
41. Nelson CE, et al. In vivo genome editing improves muscle function in a mouse model of Duchenne muscular dystrophy. *Science*. 2016;351(6271):403–407.
42. Tabebordbar M, et al. In vivo gene editing in dystrophic mouse muscle and muscle stem cells. *Science*. 2016;351(6271):407–411.
43. Young CS, et al. A single CRISPR-Cas9 deletion strategy that targets the majority of DMD patients restores dystrophin func-

tion in hiPSC-derived muscle cells. *Cell Stem Cell*. 2016;18(4):533–540.
44. Bengtsson NE, et al. Muscle-specific CRISPR/Cas9 dystrophin gene editing ameliorates pathophysiology in a mouse model for Duchenne muscular dystrophy. *Nat Commun*. 2017;8:14454.
45. Ruan GX, Barry E, Yu D, Lukason M, Cheng SH, Scaria A. CRISPR/Cas9-mediated genome editing as a therapeutic approach for Leber congenital amaurosis 10. *Mol Ther*. 2017;25(2):331–341.
46. Sanz DJ, Hollywood JA, Scallan MF, Harrison PT. Cas9/gRNA targeted excision of cystic fibrosis-causing deep-intronic splicing mutations restores normal splicing of CFTR mRNA. *PLoS ONE*. 2017;12(9):e0184009.
47. Nonaka I, Une Y, Ishihara T, Miyoshino S, Nakashima T, Sugita H. A clinical and histological study of Ullrich's disease (congenital atonic-sclerotic muscular dystrophy). *Neuropediatrics*. 1981;12(3):197–208.
48. Bertini E, Pepe G. Collagen type VI and related disorders: Bethlem myopathy and Ullrich scleroatonic muscular dystrophy. *Eur J Paediatr Neurol*. 2002;6(4):193–198.
49. Lampe AK, Bushby KM. Collagen VI related muscle disorders. *J Med Genet*. 2005;42(9):673–685.
50. Schafer S, Miao K, Benson CC, Heinig M, Cook SA, Hubner N. Alternative splicing signatures in RNA-seq data: percent spliced in (PSI). *Curr Protoc Hum Genet*. 2015;87:11.16.1–11.1614.
51. Aartsma-Rus A, et al. Guidelines for antisense oligonucleotide design and insight into splice-modulating mechanisms. *Mol Ther*. 2009;17(3):548–553.
52. Aartsma-Rus A. Overview on AON design. *Methods Mol Biol*. 2012;867:117–129.
53. Gualandi F, et al. Antisense-induced messenger depletion corrects a COL6A2 dominant mutation in Ullrich myopathy. *Hum Gene Ther*. 2012;23(12):1313–1318.
54. Bolduc V, Zou Y, Ko D, Bönnemann CG. siRNA-mediated allele-specific silencing of a COL6A3 mutation in a cellular model of dominant Ullrich muscular dystrophy. *Mol Ther Nucleic Acids*. 2014;3:e147.
55. Noguchi S, Ogawa M, Kawahara G, Malicdan MC, Nishino I. Allele-specific gene silencing of mutant mRNA restores cellular function in Ullrich congenital muscular dystrophy fibroblasts. *Mol Ther Nucleic Acids*. 2014;3:e171.
56. Marrosu E, Ala P, Muntoni F, Zhou H. Gapmer antisense oligonucleotides suppress the mutant allele of COL6A3 and restore functional protein in Ullrich muscular dystrophy. *Mol Ther Nucleic Acids*. 2017;8:416–427.
57. Donkervoort S, et al. Mosaicism for dominant collagen 6 mutations as a cause for intrafamilial phenotypic variability. *Hum Mutat*. 2015;36(1):48–56.
58. Gaudelli NM, et al. Programmable base editing of A•T to G•C in genomic DNA without DNA cleavage. *Nature*. 2017;551(7681):464–471.
59. Adikusuma F, Pfitzner C, Thomas PQ. Versatile single-step-assembly CRISPR/Cas9 vectors for dual gRNA expression. *PLoS One*. 2017;12(12):e0187236.